

Rate dependent fracture behavior of highly cross-linked epoxy resin

K. Mishra^{1,2,3}, L. Brassart^{3,4}, A. Singh^{2*}

¹IITB-Monash Research Academy, IIT Bombay, Mumbai, India – 400076

²Department of Metallurgical Engineering and Materials Science, Indian Institute of Technology, Bombay 400076

³Department of Materials Science and Engineering, Monash University, Clayton, VIC 3800, Australia

⁴Department of Engineering Science, University of Oxford, Oxford OX1 3PJ, United Kingdom

* Corresponding author: Aparna Singh, aparna_s@iitb.ac.in

Abstract

The fracture behavior of highly cross-linked epoxy resin under plane strain conditions for crack tip strain rates spanning over four orders of magnitude (10^{-4} - 10^{-1} s⁻¹) has been examined. The plane strain fracture toughness initially decreases with increasing crack tip strain rate ($\dot{\epsilon}_{tip}$) and saturates at ~ 0.8 MPa-m^{0.5} after $\dot{\epsilon}_{tip} \sim 0.02$ s⁻¹ is attained. For all the fracture specimens, a fracture process zone (FPZ) forms ahead of the sharp pre-crack prior to catastrophic failure due to the intensified stresses ahead of the crack tip. This FPZ region consists of crazes that govern the micro mechanism of fracture and this was explicitly proved using in-situ testing in a scanning electron microscope. For low strain rates, crazing in the FPZ is expected to be dominated by chain disentanglements, with craze openings more than 200 nm, whereas, chain-scission is expected to dominate at higher strain rates, with lower craze openings of ~ 150 nm.

Keywords: Fracture toughness, strain rate, epoxy, crazing

1. Introduction

Fiber-reinforced plastics are two-component material systems where flimsy yet stiff and strong fibers are held together by a polymer matrix. Thermosetting polymers such as epoxies are the polymer of choice for most high performing composites as they are easier to manufacture due to low viscosity and excellent penetration into the fiber network, leading to superior mechanical properties [1–3]. However, cross-linked epoxy matrix has a low value of fracture toughness (< 2 MPa-m^{0.5}) [4,5] and hence is extremely sensitive to the presence of flaws. Upon fatigue loading, multiple cracks nucleate in microscopically small weaker regions of the composite, which grow with time until the crack length attains a critical value, thus causing failure. The nucleation and growth of such cracks depend upon the deformation mechanisms of the epoxy matrix, the interfacial strength between fiber and matrix, and the mechanical properties of the fiber [6]. In the present work, our attention is restricted to the understanding of fracture of the epoxy matrix.

The onset of plastic deformation of epoxy on a microstructural level is envisaged as either a shear yielded “shear transformation zone” (STZ)[7–10] and/or a “craze” where a bunch of polymer fibrils is deformed by being oriented along the local tensile direction [11]. The formation of these two distinct deformation footprints can be merely a consequence of the stress state [12–14]. However, recent studies have stated that the phenomenon of deformation by shear yielding through microscopic shear band formation is the dominant mechanism in highly cross-linked epoxy resin[7,8,15]. On the other hand craze formation is favored by the high tensile stresses at the tip of a sharp crack, and a high dilatation stress component as craze matter formation is accompanied by an increase in the local volume [11,16]. However, there have been studies where there was no evidence of craze formation on fracture surfaces even in the presence of a sharp crack[15]. It is often believed that the lack of molecular mobility in highly crosslinked epoxy prevents crazing, however, there could be microscopic local regions of enhanced molecular mobility where the cross linking is less due

to impurities and imperfections in curing. These regions could exhibit crazing when suitable conditions are available such as exaggerated tensile stresses in front of a crack tip [13,14,17]. Understanding the constitutive behavior, bulk and microscopic deformation mechanisms of epoxy is necessary as they affect the fracture behavior of the composites.

Microscopy-based studies on the fracture surface of un-notched specimens have revealed that fracture initiation occurs at pre-existing defects [8,11,12]. The crack initiation is followed by a smooth slow crack propagation region which scales directly with temperature and inversely with strain rate before catastrophic failure occurs [12]. A region of crack arrest and blunting is reported prior to catastrophic failure which corresponds to the delay in reaching the failure stress [8]. However, for a notched (sharp pre-cracked) specimen, the crack initially blunts due to the formation of a plastic zone and catastrophic failure occurs on the attainment of the failure stress [8]. However, such a mechanism is prevalent for only a sharp crack with an extremely small tip radius usually obtained by tapping a sharp razor blade at the root of a machined notch. For the case of a blunt pre-crack, the tensile stresses ahead of the crack tip would interact with the pre-existing defects or weak regions of the resin and cause failure like an un-notched specimen [11]. A sharp pre-crack is essential for the proper estimation of fracture toughness as a blunt specimen (usually obtained by sawing) would result in over-estimation of fracture toughness due to notch radius-dependent toughness [18,19]. Cherry, B. W., & Thomson, K. W. [20] have studied the effect of loading rate on the fracture of epoxy systems having different yield strength using a parallel double cantilever beam specimen. They have observed a transition from a stable to unstable crack propagation as the loading rate was increased. The crack propagation was more stable for specimens with lower yield strength [20]. Kanchanomai et al. [21] have studied the effect of loading rate on fracture of epoxy but their study involved pre-cracking by sliding a razor which resulted in measurement of extremely high values of fracture toughness. They have reported that fracture toughness decreased and saturated at higher strain rates and crazes are formed ahead of the crack tip but the exact failure micromechanisms has not been reported. Marzi et al. [22] have studied the effect of loading rate on fracture toughness of adhesively bonded joints and reported an opposite trend to that reported by Kanchanomai et al. [21] for the variation of fracture toughness with loading rate. Hence, there is a lack of systematic studies that focus on the fracture of epoxy under varying loading rates and investigate the associated crack tip micromechanisms in the presence of a sharp flaw. Such studies are expected to be beneficial for estimating the balance working life of epoxy-based composites and components when the loading spectrum is well known.

In the present study, it was first proved using in-situ SEM that the epoxy used in the current study indeed failed by a crazing mechanism. Moreover, a systematic experimental investigation of the effect of strain rate on the plane strain fracture toughness of neat epoxy specimens has been conducted, which had a sharp pre-crack obtained by tapping a razor blade at the root of a machined notch. The strain rate at the crack tip was carefully measured using a video extensometer. The fracture surfaces were examined using scanning electron microscopy (SEM) and atomic force microscopy (AFM). The fracture toughness initially decreased with an increase in strain rate but saturated for higher strain rates. The fracture surface consisted of crack stretch marks left from broken craze fibrils. The density of the crack stretch marks and the broken craze fibril stretch decreased as the crack-tip strain rate increased. It is inferred that the micro-mechanism controlling fracture changes from disentanglement crazing to chain scission crazing as the strain rate is increased. Thus, caution should be exercised while testing epoxies for fracture toughness as their fracture behavior is not strain rate-independent.

2. Materials and Method

2.1. Specimen preparation

The epoxy used in the present study has been procured from Fine Finish Organics Pvt. Ltd. EPOFINE ® - 5052, which is a laminating grade low viscosity DGEBA (Bisphenol A diglycidyl ether) based epoxy cured using a polyamine hardener FINEHARD™ - 5052. The epoxy-hardener system is widely used for making large industrial and aerospace laminates. 100 parts by weight of the epoxy were mixed with 38 parts by weight of the hardener as specified by the supplier. The components were measured using a digital weighing balance having a least count of 0.0002 grams. The epoxy-hardener mixture was well stirred to ensure uniform mixing followed by vacuum degassing for 30 minutes to remove any trapped air. The degassed epoxy-hardened mixture was then poured into molds made of silicone rubber to obtain the desired specimen dimensions. The epoxy was then cured for 24 hours at 25°C followed by post-curing for 150 minutes at 100°C. The glass transition temperature (T_g) of the cross-linked epoxy was determined to be 105°C using Differential Scanning Calorimetry (DSC) technique as per ASTM D6604 – 00 [23].

2.2. Fracture toughness testing

The plane strain fracture toughness tests were done on a 1 kN capacity Instron ELECTROPULS E1000 electrically plus pneumatically actuated UTM equipped with a video-extensometer for precise measurement of strains. The specimen dimensions and test methodology were as per ASTM D5045-14 standard [24]. The specimen used for the test is shown in **Figure 1**. The molded fracture test specimens were ground using emery papers of fine grit size followed by polishing using well dispersed colloidal silica suspension in water for short durations to remove surface flaws and obtain a mirror like finish. The sample thickness (B) is maintained at 5 mm so as to ensure a plane-strain condition during testing. All other dimensions are scaled as per ASTM D5045-14 standard [24] considering B = 5 mm. The minimum thickness requirement for a valid K_{Ic} test (B) is given by

Equation 1

$$B \geq 2.5(K_{Ic}/\sigma_{YS})^2.$$

To confirm the minimum size required for a valid K_{Ic} test, tensile test was conducted for epoxy manufactured using a method as mentioned in Section 2.1. Flat tensile specimens having a gauge cross section of 6 mm x 2 mm and gauge length of 25 mm were machined followed by polishing to obtain a mirror like finish. The tensile test was conducted on a 5kN capacity pneumatically actuated UTM at a strain rate of 0.0003 s⁻¹. The engineering stress-strain plot was used to determine the yield strength using the 0.2% strain offset line and the ultimate tensile strength corresponded to the maximum stress achieved. The yield strength (σ_{YS}) and the UTS was measured to be ~55 MPa and ~ 65 MPa respectively. The σ_{YS} was used to determine B for a valid K_{Ic} test using Equation 1, which implies B must be greater than ~ 1 mm. The thickness requirement maintained in the present study is more than 5 times than that required for maintaining a plane strain condition.

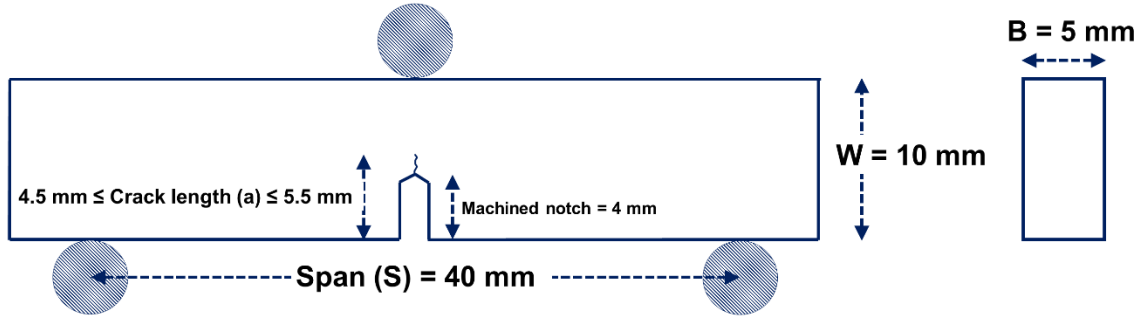


Figure 1 Dimensions of the specimen used for plane strain fracture toughness tests

The pre-cracking was done by tapping a sharp razor blade at the root of a machined notch to achieve an $0.45 \leq (a/W) \leq 0.55$ (where a is the crack length and $W = 10$ mm is the specimen width). The tapping was done carefully to ensure the growth of a uniform through thickness crack in the specimen. The crack length was measured using an optical microscope in the transmittance mode as shown in **Figure 2**. The cracks obtained were sharp and straight and in accordance with ASTM D5045-14.

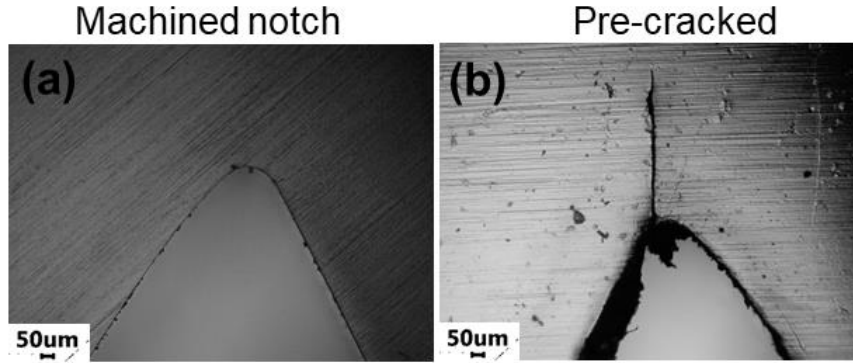


Figure 2 Specimen for the fracture toughness test (a) un-notched specimen (b) notch made by tapping sharp razor blade at the root of the machined notch

The pre-cracked specimens were subsequently tested using a three-point bend fixture and the load versus cross-head displacement plots were recorded. The peak load was then marked and the candidate fracture toughness was determined using **Equation 2** and **Equation 3**.

Equation 2

$$K_Q = \left(\frac{P_Q}{BW^{3/2}} \right) f\left(\frac{a}{W}\right)$$

Equation 3

$$f\left(\frac{a}{W}\right) = \frac{6 \left(\frac{a}{W}\right)^{0.5} \left[1.99 - \left(\frac{a}{W}\right) \left(1 - \left(\frac{a}{W}\right)\right) \left(2.15 - 3.93 \left(\frac{a}{W}\right) + 2.7 \left(\frac{a}{W}\right)^2\right) \right]}{\left[\left(1 + 2 \left(\frac{a}{W}\right)\right) \left(1 - \left(\frac{a}{W}\right)\right)^{1.5} \right]}$$

Where K_Q is the candidate fracture toughness in $\text{MPa}\sqrt{\text{m}}$, P_Q is the load at which specimen failed in kN, B is the specimen thickness in cm and W is the specimen width in cm.

The K_Q qualifies as plane strain fracture toughness if it satisfies all the conditions as listed in ASTM D5045-14 [24]. Although the ASTM D5045-14 standard mentions the cross-head velocity of 10 mm/minute, tests have been conducted at cross-head velocity ranging from 0.1 – 100 mm/minute (0.1, 1, 5, 10, 20 and 100 mm/minute) to examine the effects of loading rate on the fracture mechanisms. A minimum of six specimens have been tested for every cross-head velocity to evaluate the deviation in the results. The samples shall be referred to as CV0.10, CV001, CV005, CV010, CV020 and CV100 for specimens tested at 0.1, 1, 5, 10, 20 and 100 mm/minute cross-head velocities, respectively. To record the rate at which the specimen is strained at the crack tip due to the changing cross-head velocities, a video-extensometer is used to measure the strains by recording the displacements between two points that are placed equally spaced on both side of the crack-tip. The distance between the two points was consistently maintained between 1.1-1.2 mm. The strain rate measured for fracture toughness tests at different cross-head velocities is listed in **Table 1**.

Table 1 Cross head velocity and corresponding strain rate

Specimen name	Cross-head velocity for the fracture toughness test in mm/min	Strain rate ahead of the crack tip (exact measurement) in s^{-1}	Strain rate ahead of the crack tip in s^{-1} (rounded up)
CV0.10	0.1	$3.2 \times 10^{-4} \pm 4 \times 10^{-5}$	0.0003
CV001	1	$5.6 \times 10^{-3} \pm 3 \times 10^{-4}$	0.005
CV010	10	$1.9 \times 10^{-2} \pm 6 \times 10^{-3}$	0.02
CV100	100	$2.1 \times 10^{-1} \pm 9 \times 10^{-2}$	0.2

2.3. Fracture surface analysis

The fracture surface analysis was done using an AURIGA-ZIESS dual-beam FEG-SEM (Field Emission Gun - Scanning Electron Microscopy). The SEM specimens were coated with carbon for making the surface conductive.

2.4. Atomic force microscopy (AFM) of fracture surface features

Atomic Force Microscopy was done for the characterization of the fracture surface feature of fracture toughness specimens. A Bio-AFM MFP-3D, Asylum Research (Oxford Instruments Company) AFM operating in peak force tapping mode equipped with a Ti/Ir coated silicon tip (tip radius 28 ± 10 nm) having a spring constant of 42 N/m and a nominal resonant frequency of 300 Hz was used for the analysis. A final area of $5 \mu m \times 5 \mu m$ was scanned and the results were analyzed using the AFM software.

2.5. In-situ SEM testing of epoxy for a single edge notch tension (SENT) specimen

To understand the deformation mechanism ahead of a sharp crack and to identify the trail left by the crack tip deformation mechanism on the fracture surface, tensile test was performed in-situ SEM on a specimen in the SENT configuration. The schematic of the specimen used is shown in Figure 3(a). The single edge notch was done by tapping a sharp razor blade similar to the process of pre-cracking adopted for the fracture toughness test. The sharp pre-crack obtained by tapping a razor blade is shown in Figure 3(b). The epoxy SENT specimen was mirror polished followed by coating with carbon to make the surface conductive. The test was conducted at a crosshead velocity of 0.2 mm/minute which resulted in a strain rate of ~ 0.0007

s⁻¹ over the gauge section. The test was paused intermittently to capture the SEM micrographs. Due to the limitations of the testing set-up, the thickness of the specimen was maintained ~ 1.2 mm.

3. Results

3.1. In-situ SEM testing of epoxy using a SENT specimen

The pre-cracking of the in-situ SENT specimen using a sharp razor blade resulted in the formation of sharp pre-crack as shown in **Figure 3(c)**. As the load is increased, a small stretched region starts to form ahead of the crack (**Figure 3(d)**). This newly formed region is identified to be a crazed region which usually forms ahead of a sharp crack when the specimen is loaded. The crazed region is a region in the polymer which is like an interpenetrating web of voids and polymer fibrils. The polymer fibrils are oriented perpendicular to the craze plane (which is marked as black dotted line in **Figure 3(d)**). In spite of the presence of voids in the crazed region, they still have the capacity of bearing load. In **Figure 3(d)** some regions appear to be charged as these regions are formed newly from the bulk and hence carbon coating may not be present. At a slightly higher load (just before failure) in **Figure 3(e)**, a crack develops in this stretched region (craze region). **Figure 3(f,g,h)** shows the SEM micrographs of the fracture surface in the craze region. A uniform coverage of crack stretch marks is present on the fracture surface in the craze region. Hence, the crack stretch marks observed on the fracture surface are attributed to what remains of the stretched and broken fibrils formed inside a craze.

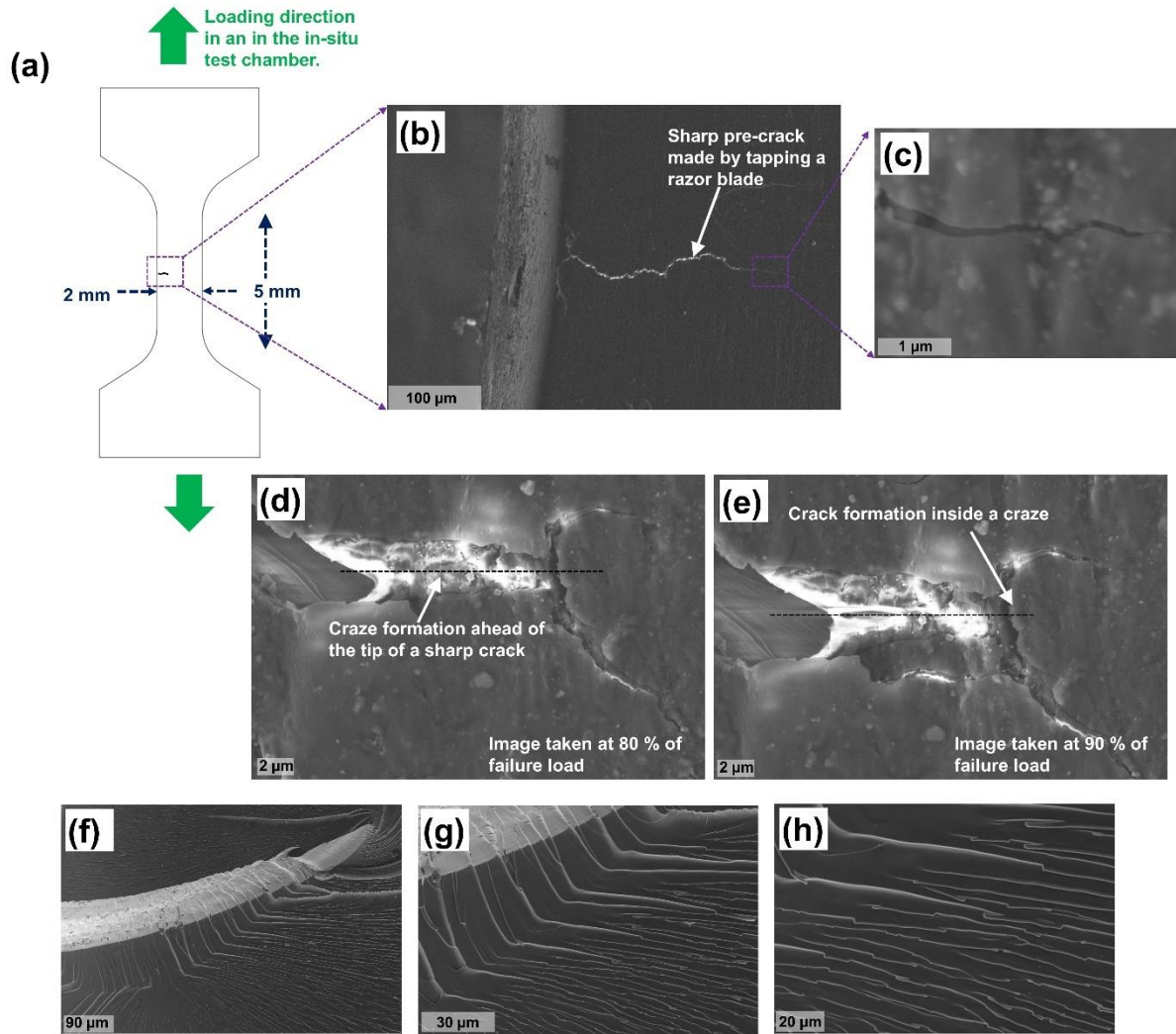


Figure 3 In-situ tensile testing of epoxy using a SENT specimen: (a) Dimension of SENT specimen used, location of pre-crack and loading direction, (b) SEM image of the sharp pre-crack, (c) high magnification SEM image of the crack tip, (d) SEM image of the craze region formed ahead of the crack tip when the load was $\sim 80\%$ of failure load, (e) SEM image showing crack formation in the craze region when the load was $\sim 90\%$ of failure load and (f,g,h) fracture surface of the SENT specimen in the crazed region. The black dotted line on (d) and (e) indicate the craze plane.

3.2. Fracture toughness test

Figure 4 shows the $\text{load} \cdot f(a/W)$ versus displacement curve obtained during the fracture toughness test carried out at different cross-head velocities. Although a minimum of 6 specimens were tested per condition, only one representative set of $\text{load} \cdot f(a/W)$ versus displacement curve is presented as shown in **Figure 4**. The load has been multiplied with the corresponding $f(a/W)$ to normalize the effect of small differences in pre-crack length and the specimen width. In all the cases, catastrophic failure happens once peak load is reached similar to a Type II kind of fracture as defined by Cherry and Thomson [20]. It is observed that the maximum $\text{load} \cdot f(a/W)$ initially decreased rapidly with an increase in cross-head velocity up to 10 mm/minute and thereafter remained more or less constant. Beyond 10 mm/minute although the $\text{load} \cdot f(a/W)$ were similar, the displacements achieved at maximum $\text{load} \cdot f(a/W)$ decreased with further increase in cross-head velocity. It is important to note that

there is no appreciable change observed in the load* $f(a/W)$ versus displacement curve before the maximum load is reached and complete failure happens.

Figure 5 shows the variation of plane strain fracture toughness (K_{Ic}) for specimens tested at different crack tip strain rates. The strain rate at the crack-tip has been measured using the method described in **Section 2.2**. The strain rates thus obtained are listed in **Table 1**. The strain rates have been presented for cross-head velocities spanning over four orders of magnitude (1×10^{-1} to 1×10^2) which resulted in strain rates also spanning over four orders of magnitude ($3 \times 10^{-4} \text{ s}^{-1}$ to $2 \times 10^{-1} \text{ s}^{-1}$). The K_{Ic} initially decreased from a high value of $0.94 \pm 0.1 \text{ MPa-m}^{0.5}$ for a crack tip strain rate of 0.0003 s^{-1} to a value of $0.79 \pm 0.09 \text{ MPa-m}^{0.5}$ for a crack tip strain rate of 0.02 s^{-1} . Thereafter, there was negligible change in K_{Ic} up to a crack tip strain rate of 0.2 s^{-1}

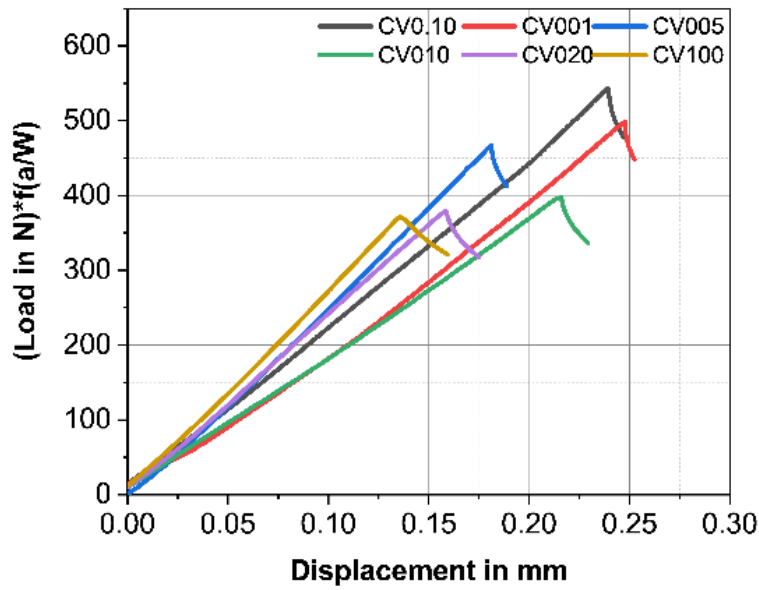


Figure 4 (Load* $f(a/W)$) versus displacement curve for fracture toughness test carried out at different cross-head velocity

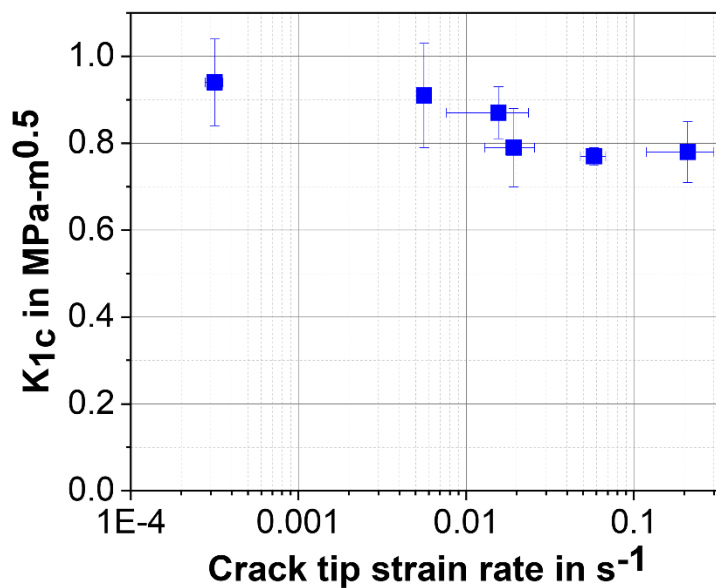


Figure 5 Variation of plane strain fracture toughness with crack tip strain rate

3.3 Fractography of fracture toughness specimen

Figure 6 shows the SEM micrographs of different regions of a typical fracture surface obtained during the fracture toughness test, starting from the root of the machined notch up to final fracture. At first, a region is observed up to which the sharp razor blade was able to travel during tapping to generate a pre-crack (Region A). The length of 'Region A' is typically between 100-300 μm . The tapping of the razor blade caused the pre-crack to extend even further which is named as 'Region B' in **Figure 6**. This region typically extends between 200-500 μm . The tapping action of the razor causes the surface to separate from the end of 'Region A' to develop 'Region B' without any further travel of the razor blade. This process allows the generation of sharp pre-crack prior to the fracture toughness test. The pre-crack process was continuously tracked using an optical microscope in the transmittance mode.

During the fracture toughness test, as load is applied, a zone is formed ahead of the sharp pre-crack which starts from the root of the pre-crack (end of 'Region B') to generate a third region (Region 'C'). 'Region C' in **Figure 6** consists of fracture feature or crack-stretch marks which are typical for a test at a particular cross-head velocity and these features are also observed to change as the cross-head velocity is changed. The features in region 'C' thus become the signature of the fracture process occurring at a particular crack tip strain rate (or cross-head velocity). Hence, region 'C' is fracture process zone (FPZ) formed ahead of the sharp pre-crack. After this point, the fracture surface appears featureless as crack tip stress field were not large enough to affect this region (Region D).

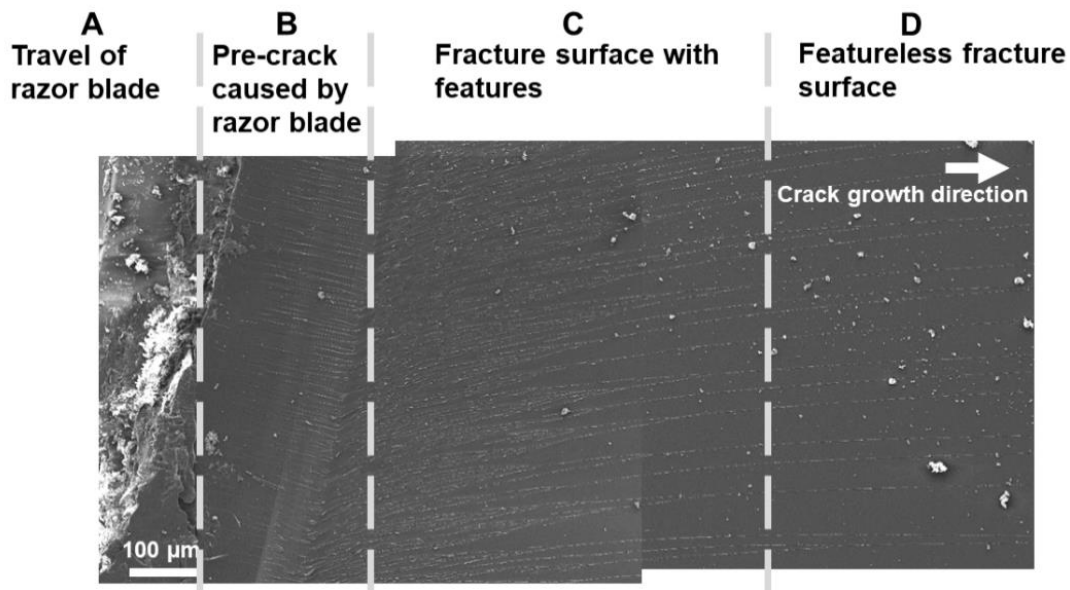


Figure 6 Typical example of different stage of fracture surface obtained from the root of the machines notch till final fracture. The fracture surface image is taken for test conducted at cross-head velocity of 5 mm/min.

Figure 7(a-l) shows the magnified SEM image of the FPZ (Region C) for samples tested at different cross-head velocities/crack tip strain rates. For all the cases, the crack stretch marks running on the fracture surface in bundles, which tend to converge along the crack propagation direction. The point of convergence of such a bundle of crack stretch marks becomes the point of initiation of new bundle of crack stretch marks on the fracture surface. The density of such crack stretch marks contained in one bundle increases with increase in cross-head velocity up to 10 mm/min and thereafter decreases with further increase in cross-

head velocity. The spacing between such bundles goes on increasing with an increase in cross-head velocity. **Figure 8** presents a schematic of the variation in the nature of formation of crack stretch marks in the FPZ (Region C) with increasing cross-head velocity for fracture toughness test. The presence of such crack stretch marks on the fracture surface is attributed to the formation of crazes formed ahead of the pre-existing sharp crack. For the fracture toughness tests, the specimen thickness was maintained such that a plane strain condition prevailed ahead of the crack tip. Along with a plane strain condition, at the tip of the crack, there are exaggerated tensile stresses promoting the formation of crazes across a plane perpendicular to the direction of tensile stresses [25]. The plane perpendicular to the tensile direction is the crack propagation plane which is presented in **Figure 7(a-l)**. Hence, it is expected that such crack stretch marks in Region 'C' are the remnant impressions of the broken craze fibrils formed ahead of the crack tip on the fracture surface after complete material separation has occurred. Although crazes are three dimensional structures, it is important to note that what is observed on the fracture surface through SEM micrographs are only two-dimensional impressions of these three-dimensional broken craze fibrils.

With an increase in the strain ahead of the crack-tip, the crazed region would ultimately fail once loading is high enough, causing catastrophic failure[26]. It is also observed that the spacing between bundles of these crack stretch marks increases with increasing cross-head velocity. For CV0.10, the crack stretch marks are uniformly spaced in the 'Region C' of the fracture surface whereas for higher cross-head velocities, the crack stretch marks start to be contained in bundles and the spacing of such bundles increases with cross-head velocity. This indicates that different regions of the epoxy have different propensity towards craze formation. The regions with higher propensity towards craze formation could be regions where the matrix is weak such as heterogeneities, microscopic regions of improper curing, dust or microscopic regions of lower cross link density etc.

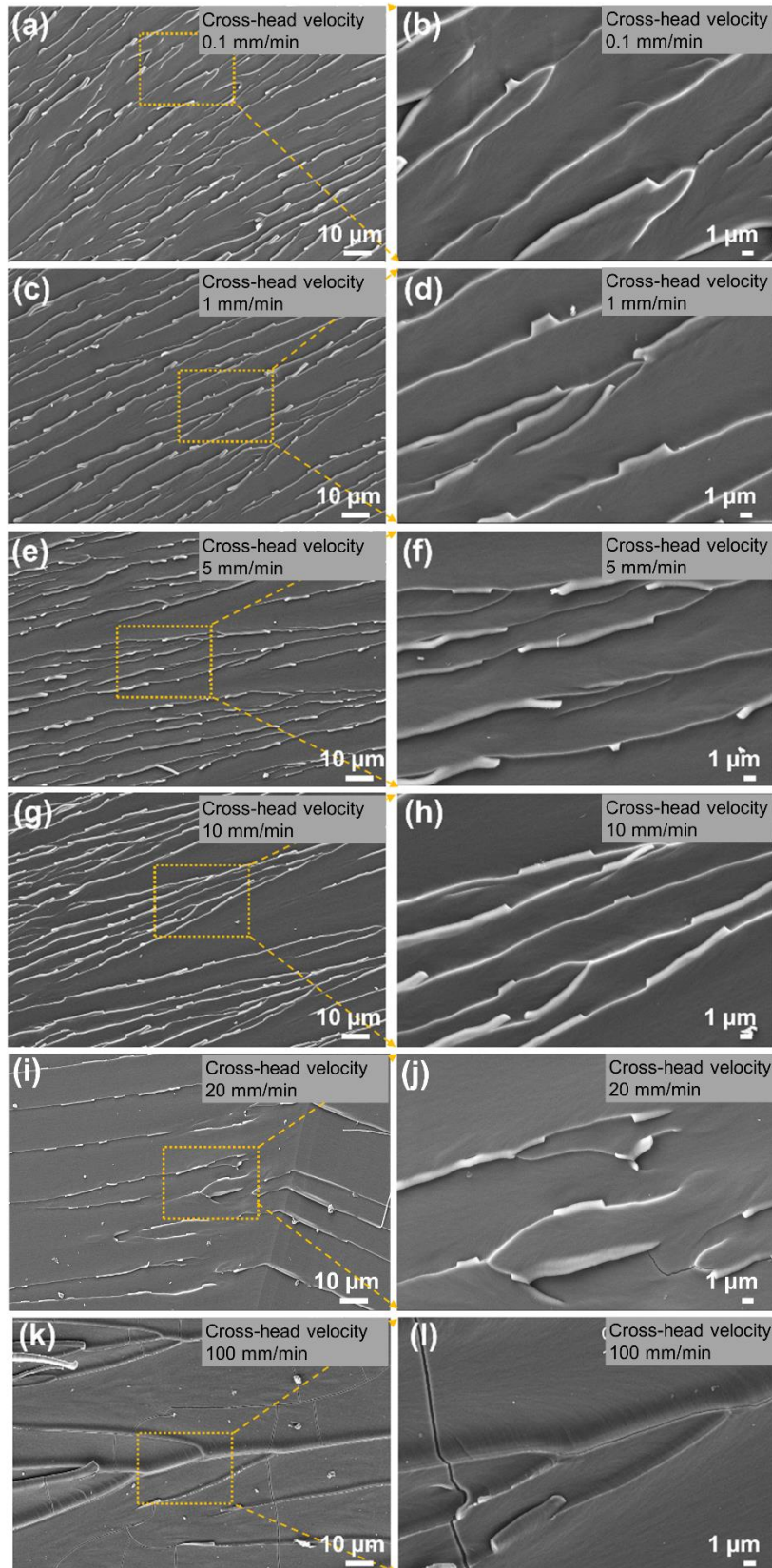


Figure 7 SEM images of fracture surface in the FPZ for the fracture toughness tested specimens at different cross-head velocity (a,b) CV0.10 (0.1 mm/min crosshead velocity) (c,d) CV001 (1 mm/min crosshead velocity) (e,f) CV005 (5 mm/min crosshead velocity) (g,h) CV010 (10 mm/min crosshead velocity) (i,j) CV020 (20 mm/min crosshead velocity) (k,l)

CV100 (100 mm/min crosshead velocity). The crack propagates from left towards right in all the micrographs.

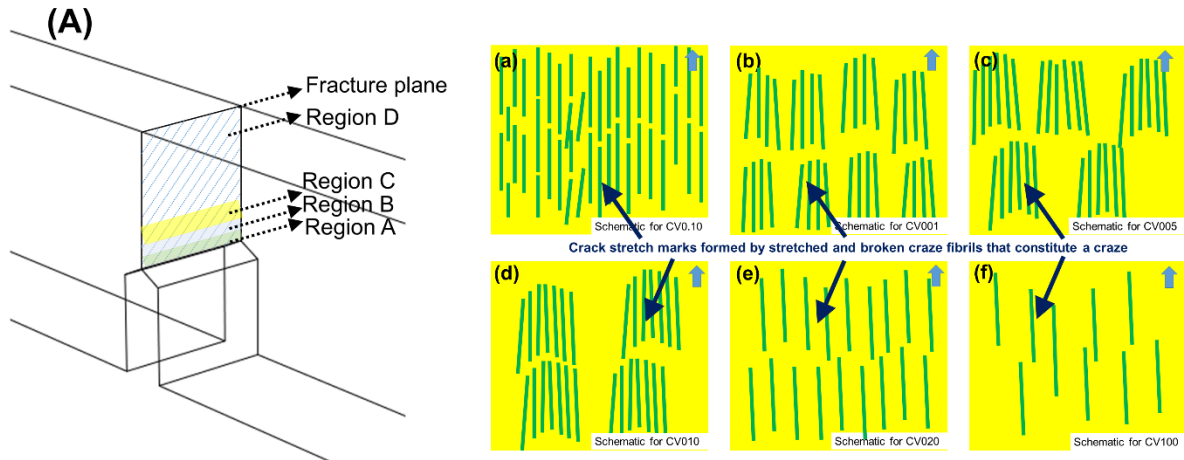


Figure 8 A two-dimensional schematic representation of the variation in the nature of crack stretch marks formed on the fracture surface in the FPZ (Region C) with increasing cross-head velocity for fracture toughness test. (A) represents the plane of fracture in a typical SENB specimen. The arrow in the top right corner of (a-f) indicates the direction of crack propagation on the fracture surface

3.4. Atomic Force Microscopy

AFM was done in the 'Region C' of the fracture toughness tested specimens. The scanned region was selected such that it contained one craze in the FPZ. A minimum of six crazes across a minimum of two specimens per condition was examined for determination of the height of broken craze fibrils after failure. It is important to note that we only record the permanent stretch that has happened in the craze and the elastic part of the stretch would be recovered after fracture. An example of the AFM micrograph of the broken craze fibril mark for specimens tested at a cross-head velocity of 0.1 mm/min (crack tip strain rate of 0.0003 s^{-1}) is presented in **Figure 9**. From the line profile of the changes in height of the FPZ as a craze is traversed, an estimate of the broken craze fibril stretch is done. This measures the stretch of the broken craze fibrils that were stretched in the craze and now relaxed. It is observed that broken craze fibril stretch decreases as the cross-head velocity (or strain rate at the crack tip) increases. This indicates that the extent to which FPZ (Region C) is stretched varies with crack tip strain rate (cross-head velocity). The K_{Ic} decreases as the broken craze fibril stretch decreases. Basing on the extent to which the craze in the FPZ (Region C) is stretched, the crazing phenomenon can be divided into two types: a high stretch craze fibrils and a low stretch craze fibrils. For cross-head velocities less than 10 mm/min, a high broken craze fibril stretch is reached, with opening between 200 -300 nm, whereas, for higher cross-head velocities, the broken craze fibril stretch decreases with opening to around 150 nm (**Figure 10**). The strain at which the final fracture occurs is expected to be proportional to the maximum stretch of the crazes. The thickness of crazes formed at all the strain rates were similar and close to $1 \mu\text{m}$ as observed from both the SEM and AFM images.

Hence, for cross-head velocities less than 10mm/min, the K_{Ic} is higher as crazes accommodate more strain before fracture. A gradual decrease in K_{Ic} happens as the cross-head velocity is increased from 0.1 mm/min to 10 mm/min (Crack tip strain rate increases from 0.0003s^{-1} to 0.02s^{-1}) as the maximum stretch of the broken craze fibrils gradually decreases. Beyond 10 mm/min, K_{Ic} decreases to the much lower value and saturates thereafter as the strain at which the craze fibrils fail also decreases and saturates. **Figure 11** presents a

schematic of the craze stretch in the FPZ just before complete material separation (critical craze opening - δ_c). The critical craze opening δ_c : for low crack tip strain rate is much higher than the critical craze opening for high crack tip strain rate. As the stretching in the craze is limited to a few hundred of nanometres and the crazing region is limited to a few hundred microns ahead of crack tip, no appreciable change is noted in the load*f(a/W) verses displacement curve (*Figure 4*) before the maximum load is reached and complete failure happens.

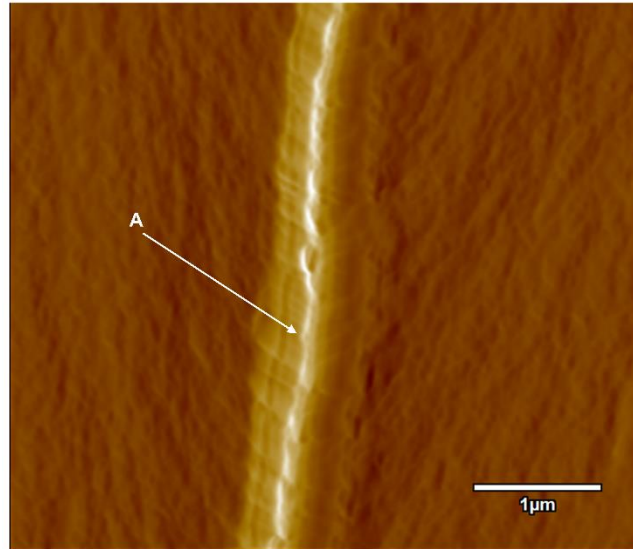


Figure 9 An example of the AFM images of a single crack stretch mark formed in in the FPZ (Region C). 'A' indicates a crack stretch mark which consist of broken craze fibrils that form a craze.

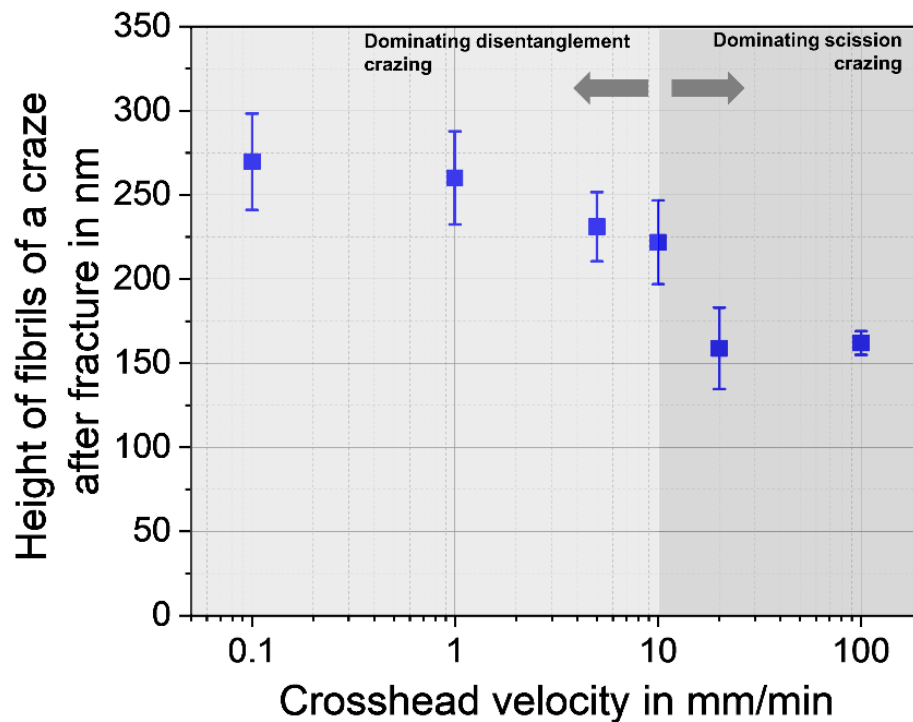


Figure 10 Variation of height of fibrils of a craze after fracture formed in in the FPZ (Region C) of fracture surface of fracture toughness tested specimens with cross-head velocity.

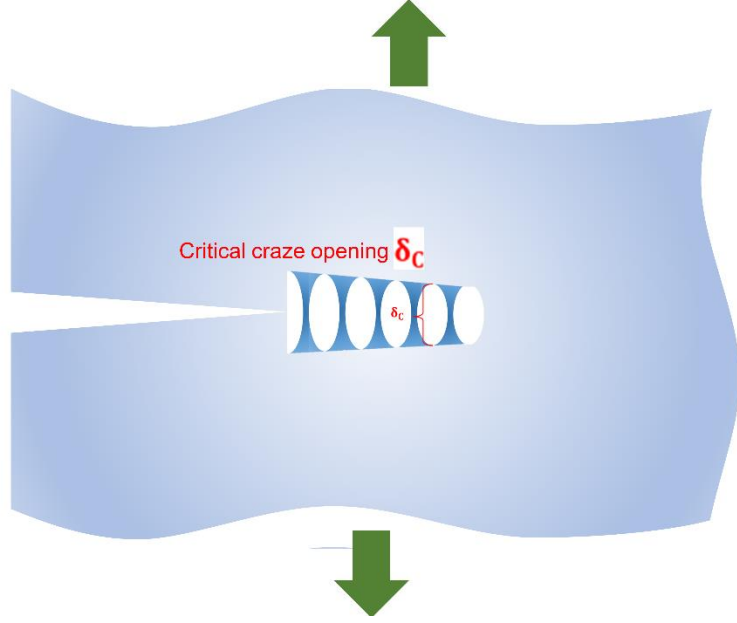


Figure 11 A schematic representation of craze stretch (stretch of fibrils within a craze) in the FPZ just before complete separation of material. The green arrow indicates that the fibrils that are in the craze, are stretched under tension.

4. Discussion

Plastic deformation preceding the failure in polymers can happen either by shear or by the formation of crazes. Shear involves the plastic deformation of a continuum, and hence no internal surfaces are created during the deformation process. Moreover, the bulk deformation process can dissipate higher energy leading to a higher toughness. On the other hand, craze requires the opening of a micro-void to generate an internal surface. The creation of an internal surface or a micro-void is facilitated by the exaggerated tensile stresses at the tip of sharp crack [25]. It is also well understood that the presence of a plane strain condition and the associated stress tri-axiality favors the formation of crazes in polymers, as is the case in the present study. Kramer and Berger [27] proposed that the formation of internal surfaces through crazing has two major contributors; the Van der Waals cohesive energy and the energy to break the covalent backbone of a polymeric chain. Hence, the energy (per unit area) for the creation of a new surface as given by Kramer and Berger [27] is presented in Equation 4.

Equation 4

$$\Gamma = \gamma_{vdw} + \frac{1}{4}v_n U$$

Here Γ is the energy for internal surface generation, γ_{vdw} is the Van der Waals cohesive surface energy, v_n is the density of strands in the network and U is the energy for breaking of the covalent bond of the polymeric backbone. The relative contributions of these two terms vary depending upon the test conditions and material properties [25,27,28]. The material properties can be varied by changing the degree of cross-link, molecular weight, chain length, varying proportions of epoxy and hardener, nano/micro filler addition and varying curing cycles. However, in the present study, the specimens have been prepared by maintaining similar conditions, and hence similar chemical properties are expected. The only test condition that is varied across the six sets of specimens in the fracture toughness tests is the cross-head velocity which manifests as a change in the strain rate at the crack tip.

From **Figure 7** it is evident that ahead of the sharp pre-crack, the formation of a FPZ containing crazes precedes catastrophic failure. The mechanism involved in the creation and breakdown of these crazes ultimately determines the fracture toughness of the specimens. However, the process of formation of craze and the type of craze is a function of both strain rate and temperature. At a lower strain rate (or high temperature), it is speculated that crazing in polymers is dominated by disentanglement crazing where polymer chains are allowed to reptate and the load is dissipated as disentanglements. Thus, in this case, the surface energy for internal surface creation is dominated by the Van der Waals cohesive forces [27,28]. On the other hand, at a high strain rate (or low temperature), both reptation of polymer chains and disentanglement becomes difficult, and crazing is suspected to occur by chain scission of polymer backbone [27,28]. Thus, at low strain rates, the energy for internal surface creation is expected to be dominated by γ_{vdw} term in **Equation 4**, whereas as crack tip strain rate increases, both parts of **Equation 4** contribute to the energy for internal surface creation while the contribution of γ_{vdw} decreases as crack tip strain rate increases.

A ‘tube model’ is often used to understand the change in the nature of crazing in polymers which is based on a critical force criterion [28]. In this model, each polymer chain is surrounded by an imaginary tube, and the frictional resistance offered by the imaginary tube is related to the constraining forces provided by the surrounding polymer network. Thus, disentanglement occurs when the frictional forces acting on the chain are weak, and chain scission happens when frictional forces exceed the chain-breaking force. Also, a smaller frictional force at lower strain rates would indicate a larger stretch of crazes. In the present study, a decrease in the craze stretch with increasing cross-head velocity of fracture toughness specimens could be due to an increase in the scission crazing mechanism of fracture. However, as indicated in **Figure 10**, a distinct change in the stretch of broken craze fibrils is observed after cross-head velocity reaches 10 mm/min. Hence, disentanglement crazing is expected to be dominant at lower cross-head velocities (or crack tip strain rates), whereas scission crazing is expected to be dominant at higher strain rates.

For the fracture toughness test, as varying strain rates are achieved (spanning over four orders of magnitudes) in front of the crack tip, the dominance of the disentanglement crazing and scission crazing is expected to vary over the six sets of specimen tested. **Figure 7** (a,b) shows that the crack stretch marks are present uniformly throughout the specimen. The point at which two such crack stretch marks terminate becomes the point of origin of new crack stretch mark. Whereas for higher cross-head velocities, the crack stretch marks appear in bundles. The spacing of such bundles increases up to a cross-head velocity of 10 mm/min (or 0.02 s^{-1} strain rate) and new crazes originate from the point of termination of such bundles of crazes. This indicates the plastic deformation becomes localized as the cross-head velocity for the fracture toughness test is increased from 0.1 to 10 mm/min (or strain rate up to 0.02 s^{-1}) as presented schematically in **Figure 8**. Also, it indicates that the volume of material participating in energy dissipation decreases as the cross-head velocity for the fracture toughness test increases from 0.1 to 10 mm/min, which leads to an initial decrease in the fracture toughness value. The uniform distribution of crack stretch marks formed from broken craze fibrils in **Figure 7**(a,b) suggests that all the regions contained in the FPZ ahead of the crack tip have an equal probability of forming crazes. This indicates that there is a higher probability of disentanglements dominate crazing as such a process would depend more on the Van der Waals cohesion between molecules, which is similar throughout the bulk of the specimen. For higher cross-head velocities **Figure 7** (c-h), the crack stretch marks and hence the broken craze fibril marks selectively appear over the fracture surface, and the broken craze fibrils have a lower value of craze stretch. Thus, the initial decrease in fracture toughness up

to a cross-head velocity of 10 mm/min is due to the reduction in the actual area contributing to energy dissipation and the decreasing strain accommodating ability of crazes.

At higher cross-head velocity (20 mm/min and 100 mm/min), the K_{Ic} saturates, the spacing between the crazes formed at the crack tip ('Region C') increases and the stretch of the crazes also saturates. As the craze stretch saturates, the K_{Ic} also saturates, and the dominant mechanism of craze failure is expected to be through chain scission. At high crack tip strain rate, the disentanglement of chains would be difficult, and fracture can occur through the breaking of covalent bonds. Hence, the fracture toughness in highly cross-linked epoxy is determined by the 'strain before failure' that the crazes formed in the FPZ ahead of the crack tip can attain. However, experimental determination of the exact contribution of disentanglement crazing and scission crazing is not been a part of this study and still remains open for research.

5. Conclusion

Fracture toughness of highly cross-linked epoxy changes with crack tip strain rate while different mechanisms of crack tip crazing are expected in the low and high strain rate regimes. The following conclusions have been made in this study

- 1) A craze region is formed ahead of a sharp pre-crack upon loading and catastrophic failure happens on attainment of a critical craze stretch. The fracture surface of craze region (FPZ) consists of crack stretch marks which are impressions of what remains of the craze fibrils formed in the craze region.
- 2) The plane strain fracture toughness of epoxy initially decreases with an increase in crack tip strain rate up to 0.02 s^{-1} and thereafter remains constant up to a strain rate of 0.2 s^{-1} .
- 3) The fracture toughness is controlled by FPZ formed ahead of the sharp crack tip. The FPZ consisted of crazes which control the fracture mechanism. The stretch of the broken fibrils in crazes gradually decreased up to a crack tip strain rate of 0.02 s^{-1} where after there is a sudden decrease and subsequent saturation in the stretch of craze fibrils. This is attributed to a possible change in the mechanism of craze formation.
- 4) An initial decrease in-plane strain fracture toughness with crack tip strain rate is attributed to an increasing in the spacing between crazes leading to localized deformation and a decrease in the strain accommodating ability of crazes.
- 5) Saturation of the fracture toughness for higher crack tip strain rate is attributed to a dominating strain-independent craze failure mechanism where craze failure is expected to be due to chain scission.
- 6) Care must be taken while conducting a plane strain fracture toughness test on epoxies as the measured value of K_{Ic} is sensitive to the loading rate.

Acknowledgment

A.S and K.M thank the Bio- AFM facility, BSBE, Industrial Research and Consultancy Center (IRCC), IIT Bombay and Mr. Vijay Mistari for the help in the AFM experiments. We would also like to acknowledge the efforts of Mr. Devyanshu Bansal who joined as a research intern in the Nano Engineering Lab (Department of Metallurgical Engineering and Materials Science, IIT Bombay) and assisted in the fracture toughness test.

References

- [1] J.D. Muzzy, A.O. Kays, Thermoplastic vs. thermosetting structural composites, Polym. Compos. 5 (1984) 169–172. <https://doi.org/10.1002/pc.750050302>.
- [2] K. Srinivasan, W.C. Jackson, B.T. Smith, J.A. Hinkley, Characterization of Damage Modes in Impacted Thermoset and Thermoplastic Composites, J. Reinf. Plast. Compos. 11 (1992) 1111–1126.

- <https://doi.org/10.1177/073168449201101004>.
- [3] I.Y. Chang, J.K. Lees, Recent Development in Thermoplastic Composites: A Review of Matrix Systems and Processing Methods, *J. Thermoplast. Compos. Mater.* 1 (1988) 277–296. <https://doi.org/10.1177/089270578800100305>.
 - [4] M. Zamanian, M. Mortezaei, B. Salehnia, J.E. Jam, Fracture toughness of epoxy polymer modified with nanosilica particles: Particle size effect, *Eng. Fract. Mech.* 97 (2013) 193–206. <https://doi.org/10.1016/j.engfracmech.2012.10.027>.
 - [5] G. Levita, S. De Petris, A. Marchetti, A. Lazzeri, Crosslink density and fracture toughness of epoxy resins, *J. Mater. Sci.* 26 (1991) 2348–2352. <https://doi.org/10.1007/BF01130180>.
 - [6] B.D. Agarwal, L.J. Broutman, K. Chandrashekara, Analysis and Performance of Fiber Composites Third Edition, 2006.
 - [7] X. Morelle, Mechanical Characterization and Physics-Based Modeling of a Highly-Crosslinked Epoxy Resin, 2015.
 - [8] J. Chevalier, X.P. Morelle, P.P. Camanho, F. Lani, T. Pardoen, On a unique fracture micromechanism for highly cross-linked epoxy resins, *J. Mech. Phys. Solids.* 122 (2019) 502–519. <https://doi.org/10.1016/j.jmps.2018.09.028>.
 - [9] J. Chevalier, L. Brassart, F. Lani, C. Bailly, T. Pardoen, X.P. Morelle, Unveiling the nanoscale heterogeneity controlled deformation of thermosets, *J. Mech. Phys. Solids.* 121 (2018) 432–446. <https://doi.org/10.1016/j.jmps.2018.08.014>.
 - [10] K. Mishra, A. Singh, Effect of strain rate on the uni-axial stress-strain behavior of highly cross-linked epoxy resin, *Procedia Struct. Integr.* 41 (2022) 248–253. <https://doi.org/10.1016/j.prostr.2022.05.028>.
 - [11] S. Bandyopadhyay, Review of the microscopic and macroscopic aspects of fracture of unmodified and modified epoxy resins, *Mater. Sci. Eng. A.* 125 (1990) 157–184. [https://doi.org/10.1016/0921-5093\(90\)90167-2](https://doi.org/10.1016/0921-5093(90)90167-2).
 - [12] R.J. Morgan, E.T. Mones, W.J. Steele, Tensile deformation and failure processes of amine-cured epoxies, *Polymer (Guildf)*. 23 (1982) 295–305. [https://doi.org/10.1016/0032-3861\(82\)90320-2](https://doi.org/10.1016/0032-3861(82)90320-2).
 - [13] W. Zhang, I. Srivastava, Y.F. Zhu, C.R. Picu, N.A. Koratkar, Heterogeneity in epoxy nanocomposites initiates crazing: Significant improvements in fatigue resistance and toughening, *Small.* 5 (2009) 1403–1407. <https://doi.org/10.1002/sml.200801910>.
 - [14] J. Lilley, D.G. Holloway, Crazing in epoxy resins, *Philos. Mag.* 28 (1973) 215–220. <https://doi.org/10.1080/14786437308217443>.
 - [15] S. Yamini, R.J. Young, The mechanical properties of epoxy resins, *J. Mater. Sci.* 15 (1980) 1823–1831. <https://doi.org/10.1007/BF00550603>.
 - [16] L.E. Asp, L.A. Berglund, R. Talreja, A criterion for crack initiation in glassy polymers subjected to a composite-like stress state, *Compos. Sci. Technol.* 56 (1996) 1291–1301. [https://doi.org/10.1016/S0266-3538\(96\)00090-5](https://doi.org/10.1016/S0266-3538(96)00090-5).
 - [17] H.J. Sue, Craze-like damage in a core-shell rubber-modified epoxy system, *J. Mater. Sci.* 27 (1992) 3098–3107. <https://doi.org/10.1007/BF01154125>.
 - [18] Y. Qiao, M. Salviato, Strength and cohesive behavior of thermoset polymers at the microscale: A size-effect study, *Eng. Fract. Mech.* 213 (2019) 100–117. <https://doi.org/10.1016/j.engfracmech.2019.03.033>.
 - [19] K. Xiao, L. Ye, Y.S. Kwok, Effects of pre-cracking methods on fracture behaviour of an Araldite-F epoxy and its rubber-modified systems, *J. Mater. Sci.* 33 (1998) 2831–2836. <https://doi.org/10.1023/A:1017533819817>.
 - [20] B.W. Cherry, K.W. Thomson, The fracture of highly crosslinked polymers - Part 1 Characterization and fracture toughness, *J. Mater. Sci.* 16 (1981) 1913–1924. <https://doi.org/10.1007/BF00540640>.
 - [21] C. Kanchanomai, S. Rattananon, M. Soni, Effects of loading rate on fracture behavior and mechanism of thermoset epoxy resin, *Polym. Test.* 24 (2005) 886–892. <https://doi.org/10.1016/j.polymertesting.2005.06.006>.

- [22] S. Marzi, O. Hesebeck, M. Brede, F. Kleiner, A rate-dependent cohesive zone model for adhesively bonded joints loaded in mode I, *J. Adhes. Sci. Technol.* 23 (2009) 881–898. <https://doi.org/10.1163/156856109X411238>.
- [23] D.S. Calorimetry, Standard Practice for Glass Transition Temperatures of Hydrocarbon Resins by Differential Scanning Calorimetry 1, 00 (2012) 1–4. <https://doi.org/10.1520/D6604-00R09E01.2>.
- [24] ASTM, (ASTM D 5054) - Standard Test Methods for Plane-Strain Fracture Toughness and Strain Energy Release Rate of Plastic Materials, ASTM B. Stand. 99 (2013) 1–9. <https://doi.org/10.1520/D5045-14.priate>.
- [25] R.A.C. Deblieck, D.J.M. van Beek, K. Remerie, I.M. Ward, Failure mechanisms in polyolefines: The role of crazing, shear yielding and the entanglement network, *Polymer (Guildf)*. 52 (2011) 2979–2990. <https://doi.org/10.1016/j.polymer.2011.03.055>.
- [26] T. Nishiura, In Situ SEM Observation of Fracture Processes in Thin Film of Poly(methyl methacrylate) II. Stress Measurement, *Polym. J.* 35 (2003) 76–78. <https://doi.org/10.1295/polymj.35.76>.
- [27] E.J. Kramer, L.L. Berger, Fundamental processes of craze growth and fracture, in: *Crazing Polym. Vol. 2*, Springer Berlin Heidelberg, Berlin, Heidelberg, 1990: pp. 1–68. <https://doi.org/10.1007/BFb0018018>.
- [28] C.J.G. Plummer, A.M. Donald, Disentanglement and crazing in glassy polymers, *Macromolecules*. 23 (1990) 3929–3937. <https://doi.org/10.1021/ma00219a011>.